

RESEARCH ARTICLE | FEBRUARY 01 2000

Effects of shallowness on the development of free-surface mixing layers

W. S. J. Uijttewaai; R. Booij



Physics of Fluids 12, 392–402 (2000)

<https://doi.org/10.1063/1.870317>



Export
Citation

CrossMark

Articles You May Be Interested In

Recirculation zone downstream lateral expansions of open channel flow

Physics of Fluids (November 2020)

Vortex formation in shallow flows

Physics of Fluids (March 2008)

Turbulent mixing and passive scalar transport in shallow flows

Physics of Fluids (January 2011)




APL Quantum

Bridging fundamental quantum research with technological applications

Now Open for Submissions

No Article Processing Charges (APCs) through 2024

Submit Today



Effects of shallowness on the development of free-surface mixing layers

W. S. J. Uijttewaala^{a)} and R. Booij

Delft University of Technology, Department of Civil Engineering, P.O. Box 5048, 2600 GA Delft, The Netherlands

(Received 12 April 1999; accepted 14 October 1999)

The development of two shallow mixing layers with different water depths is analyzed experimentally by means of laser Doppler anemometry. The experiments show that bottom friction plays an important role in the growth of the mixing layer width and in the strength and dimensions of the large quasi two-dimensional turbulence structures therein. It is found in this study that the initial growth rate of both mixing layers is similar to what has been found for deep water plane mixing layers. Further downstream the reduction of the growth rate can be ascribed to the decrease of the velocity difference between the two ambient streams in combination with the suppression of the growth of the large turbulence structures. In the most shallow mixing layer considered, the influence of the bottom friction is dominant, impeding the further growth of the mixing layer width. It is demonstrated that the reduced mixing layer growth is related to a loss of coherence in the large turbulence structures. This loss of coherence also reduces the characteristic length-scale that establishes the lateral mixing of matter and momentum in the mixing layer. Eventually the water depth becomes the dominant length scale that determines the characteristic motion of the turbulence in that case. From the energy density spectra of the turbulence fluctuations and from the phase relation between the two velocity components in the horizontal plane it is concluded that large structures contribute most to the exchange of momentum in the mixing layer and thus to the Reynolds-stresses. © 2000 American Institute of Physics. [S1070-6631(00)00502-X]

I. INTRODUCTION

Mixing layers have been the topic of turbulence research for many decades. The plane mixing layer has attained great interest, since it is the prototype of an essentially unstable flow where the instabilities lead to the formation of eddy structures.¹ Apart from the interesting physical phenomena occurring in a mixing layer, it plays an important role in the exchange of mass and momentum in many practical situations where two flows of different velocity get into contact.

In the natural environment most flows in rivers and coastal areas can be considered as shallow, i.e., the width of the flow is much larger than the water depth. The presence of a bottom and the associated effects of friction make shallow flows belonging to a special class of flows. Especially when these flows are subjected to lateral shear like in mixing layers, wakes and jets, the development of the flow is highly affected by the shallowness.^{2,3} Mixing layers develop for instance at harbour entrances, groyne fields and flood plains, between the main fast flowing stream and a recirculation zone. The horizontal exchange of momentum and mass, including contaminants, sediment and silt, is mediated by the mixing layer. Knowledge of mixing layer development under shallow conditions is of key importance regarding the prediction of shallow flows, sediment transport and erosion, and the transport of pollutants. The specific modeling aspects of shallow shear flows have been well recognized by a number of researchers which has led to improved modeling tools.^{4,5}

In these models a distinction is made between the effective “turbulence viscosity” associated with the large (quasi two-dimensional) horizontal turbulence structures that are generated in the regions of horizontal shear, and the turbulence viscosity associated with the small scale turbulence generated in the bottom boundary layer. In order to validate such models and to adjust the modeling constants to proper values, experimental data representing the most important features of shallow flows with shear are invaluable.

Though detailed experiments have been performed regarding the large turbulence structures in shallow jets and wakes,^{3,6} the shallow mixing layer has been examined less extensively.⁷ In a previous paper⁸ experimental data were presented on the development of the first two meters of a shallow mixing layer in water of 67 mm depth. It was concluded in that paper that the initial growth rate of the shallow mixing layer was similar to that of a deep water mixing layer. The influence of bottom friction on the development of the mixing layer width was not studied. In the present paper a more comprehensive set of experimental data is presented including data obtained further downstream where the shallowness does affect the mixing layer development. In the same set-up experiments have been performed using a smaller water depth of 42 mm where the influence of shallowness is even more pronounced. In addition to previous work on shallow mixing layers by other authors,⁷ we could observe the existence and development of large quasi two-dimensional turbulence structures under two different conditions of bottom friction.

^{a)}Electronic mail: W.Uijttewaal@ct.tudelft.nl

A. Mixing layer development

1. Deep-water mixing layer

In a deep-water or plane mixing layer the velocity difference and the associated gradient between two streams is a source of turbulent kinetic energy. Due to the geometry of the flow at first instance two-dimensional turbulence structures are generated. The nice pictures of the two-dimensional eddies from the experiments of Brown and Roshko⁹ are well known. The two-dimensionality of the flow leads to an organization into larger structures by means of the vortex pairing mechanism.¹⁰ Further downstream the two-dimensional structures become unstable and disintegrate into three-dimensional turbulence.¹¹

From the phenomenology of self-similar lateral velocity profiles it can be deduced that the width δ of a two-dimensional plane mixing layer grows at a constant rate.¹² This has been confirmed by numerous experiments. Here δ is defined as the maximum slope thickness, i.e.,

$$\delta = \frac{u_1 - u_2}{(\partial u / \partial y)_{\max}}. \quad (1)$$

The growth rate appears, for most experimental conditions, to be proportional to the characteristic mixing layer parameter $\lambda = (u_1 - u_2) / (u_1 + u_2)$, where u_1 , and u_2 are the streamwise velocities of the undisturbed streams

$$\frac{d\delta}{dx} = \alpha_{dw} 2\lambda. \quad (2)$$

The constant of proportionality α_{dw} , where the subscript *dw* denotes ‘‘deep water,’’ has an empirically determined constant value of about 0.09 in most cases. Exceptions to the rule are: Forced mixing layers,¹³ mixing layers with laminar boundary layers at the splitter plate,¹⁴ and shallow mixing layers.⁷ In all cases boundary conditions in the initial region at the splitter plate appear to be of great importance in the initial growth rate and the downstream development of the mixing layer.⁸

2. Shallow-water mixing layer

A very important aspect of shallowness is the additional friction caused by the presence of the bottom. This friction is responsible for the decrease of the mixing layer growth rate. The conditions for self similarity are not fulfilled since the velocity difference between both sides of the mixing layer is not constant anymore due to friction. Moreover the mixing layer width is not the only characteristic length scale, since the water depth is now restricting the turbulence motion in the vertical direction.

The effects of shallowness and the consequent bottom friction on the development of a shear layer can be expressed by a single parameter: The wake stability parameter or the bed-friction number S .¹⁵ This number is defined as the ratio between the stabilizing effect of bed friction (dissipation of turbulent kinetic energy) and the destabilizing effect of transverse shear (production of turbulent kinetic energy).² For the shallow mixing layer the bed-friction number is defined as

$$S = \frac{c_f}{2\lambda} \frac{\delta}{h}, \quad (3)$$

where h is the water depth and c_f the bottom friction coefficient.

Stability analyses have proven the existence of a critical value S_c .^{2,16} For $S \ll S_c$ the bottom friction has negligible effect and the growth of the instabilities in the mixing layer is not hindered. In case $S > S_c$ the growth of instabilities is impeded by bottom friction and its associated additional dissipation. The value of S_c for a mixing layer is found to lie between 0.06 and 0.12.^{15,17} From their experimental data Chu & Babarutsi⁷ determined for S_c a value of 0.09. Apart from friction itself the bottom shear layer might induce secondary circulation⁶ or so-called Ekman suction¹⁸ which could affect the development of large horizontal turbulence structures.

A second consequence of shallowness is the geometrical restriction of the water motion. Eddies with dimensions larger than the water depth can only move in the horizontal plane. The limited depth prohibits these eddies to be stretched in the vertical direction and forces the large eddies into a quasi two-dimensional motion. The only mechanism that can affect the large eddies, not so effective regarding energy dissipation, is the vertical velocity gradient in combination with the small scale three-dimensional turbulence.

The experimental results presented in this paper throw more light on the effects of shallowness on the large turbulent structures in the flow and its consequent impact on the mixing layer development. Data concerning the mixing layer growth rate are compared with earlier experiments of Chu and Babarutsi⁷ and scaling aspects are also discussed. Furthermore we will have a closer look at the coherence of the structures that are formed in the mixing layer. Their characteristic length scale, vertical extension, and two-dimensionality are of importance in modeling the mixing properties of such flows.

II. EXPERIMENTAL SETUP

The mixing layers are generated in a horizontal glass bottom flume, 3 m wide and 20 m long, located at the Laboratory for Fluid Mechanics at Delft University of Technology. Two shallow mixing layers are studied with different upstream water depths of 67 and 42 mm. A top view of the flume is shown schematically in Fig. 1. The inlet section of the flume consists of two separate parts divided by a splitter plate where the flows of the high and low velocity side of the mixing layer are introduced via a contraction into the horizontal part of the flume. The flow rates in both sides of the flume are adjusted using two separate valves. In the horizontal inlet part both streams are separated by a splitter plate of 3 m length ensuring the bottom boundary layers to be fully developed before the end of the splitter plate is reached.

The conditions realized at the apex of the splitter plate are given in Table I, where the subscript 0 is used to denote the inflow conditions. It is clear that the difference in water depth causes the major differences in Reynolds number, $Re = Uh/\nu$, and friction coefficient. The latter is determined

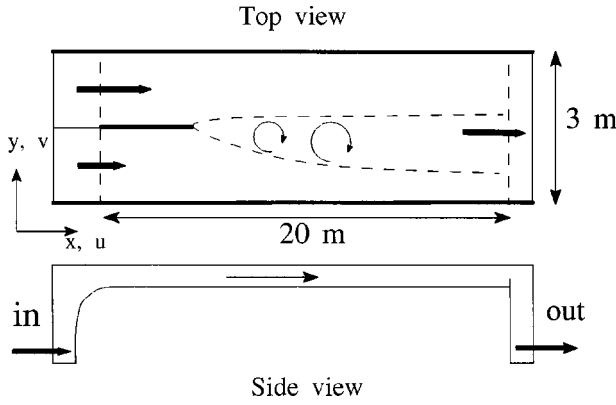


FIG. 1. Schematic view of the 20 m long, 3 m wide flume with the boundaries of the mixing layer indicated by dashed lines. Inserted axes define directions of coordinates and velocities.

from the mean flow velocity of the two streams [according to Eq. (4) in the next section]. The mixing layer parameter λ_0 at the inflow is almost equal for both situations, allowing for a proper comparison with the water depth as the most important varying parameter. The Froude number $Fr = U/\sqrt{gh}$ is much smaller than one in both cases ensuring the flow not to be affected by surface disturbances.

The smooth glass bottom of the flume, positioned at an elevation of 1.8 m above the laboratory floor, allows for optical access from below. Velocities in the horizontal plane are measured by means of Laser Doppler Anemometry (LDA) using a DANTEC fiber-optic backscatter system with two independent probes. A schematic drawing of the probe configuration is given in Fig. 2. Both probes are mounted on an automated translation stage and can be moved independently with positioning accuracy of a few micrometers. The most important positioning error is determined by misalignment of the traversing system with respect to the flume and misalignment of the probes with respect to each other. The two-component probe is mounted vertically providing a direct determination of the velocity vector in the horizontal plane, $[u, v]$. The single-component probe, measuring the v -component, is mounted at an inclination with respect to the vertical direction such that its probing volume can be made to coincide with those of the other probe. By displacing the probes, with respect to each other, spatial correlation functions of velocity fluctuations could be determined.

The Doppler signal was processed by means of a burst spectrum analyser. For each position about 10^5 bursts were detected in a time interval of 10 min. The 10 min. interval has been chosen to ensure averaging over a sufficiently large number of eddy structures. The nonequidistant data were re-sampled into equidistant data using linear interpolation after low-pass filtering. The resample frequency was 100 Hz, well

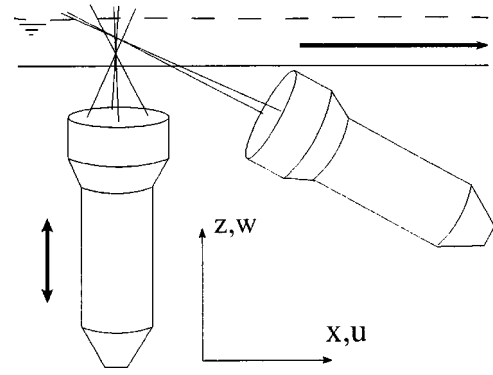


FIG. 2. Schematic drawing of LDA probe configuration used for correlation with vertical separation. Inserted axes define directions of coordinates and velocities.

below the mean sample frequency of about 166 Hz. The thus obtained equidistant data set was used to determine correlation functions, and power-density spectra.

III. EXPERIMENTAL RESULTS

Using the setup described above, experiments have been performed on two mixing layers with different depths. First the general properties of the mixing layer will be presented followed by a more detailed analysis of the turbulence and its structures in the mixing layer.

As a consequence of the initial velocity difference a mixing layer starts to develop beyond the end of the splitter plate. The development of the mixing layer and of the two undisturbed streams in the downstream direction, is affected by bottom friction and the slope of the free surface. The latter turns out not to vary with lateral position so both streams are subjected to the same forcing by the free surface slope. The bottom friction depends on the local Reynolds number. The fast stream experiences a larger friction than the slow stream resulting in a decrease of the velocity difference with downstream distance. The growth of the mixing layer width will therefore be affected by the bottom friction in two ways. First the decreasing velocity difference leads to a decreasing value of λ and in principle to a decreasing growth rate. Second, the hydrodynamical (Kelvin–Helmholtz) instabilities that govern the mixing layer growth are suppressed by the bottom friction. The friction stress at the bottom $\tau_b = -\rho c_f \bar{U} |\bar{U}| \equiv -\rho u^* |u^*|$ is dependent on the bed-friction coefficient c_f , which for a logarithmic velocity profile and a smooth bottom with roughness coefficient $z_0 = 0.135 \nu / u^*$ is obtained as

$$\frac{1}{\sqrt{c_f}} = \frac{1}{\kappa} (\ln(\text{Re} \sqrt{c_f}) + 1.0), \quad (4)$$

where κ is the von Karman constant (0.4), and $\text{Re} = \bar{U}h/\nu$ the local Reynolds number, with \bar{U} the depth averaged velocity, h the water depth, and ν the kinematic viscosity. This yields, apart from a factor of 2 due to the definition of τ_b , friction coefficients equivalent to those used by Chu and Babarutsi.^{7,19} The influence of the bed friction is known from laboratory experiments on shallow wake flows,¹⁶ shear

TABLE I. Experimental conditions at the end of the splitter plate.

	h_0 (mm)	$U_{1,0}$ (m/s)	$U_{2,0}$ (m/s)	λ_0	Re_{10}	Re_{20}	c_f	Fr_0
I	42	0.11	0.23	0.36	4600	9600	0.0033	0.28
II	67	0.14	0.32	0.40	9400	21400	0.0027	0.28

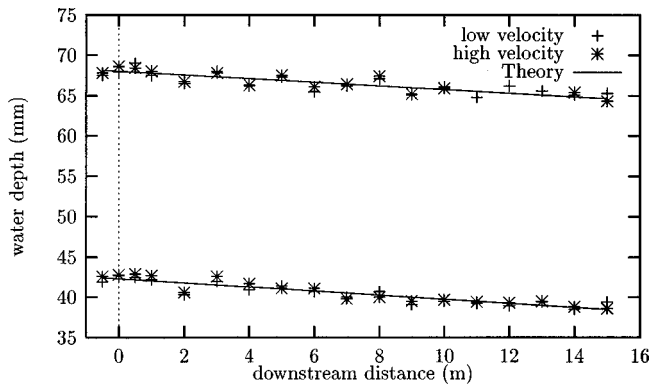


FIG. 3. Decrease of the water depth, measured at the low and high velocity side for both mixing layers, compared with prediction. The downstream distance is defined with respect to the end of the splitter plate.

layers,⁷ and jets.⁶ The flow over the horizontal bottom is maintained by a decrease of the water level with downstream position. For the mean flow through the flume we can write for the one-dimensional depth averaged continuity and momentum equation

$$\frac{d\bar{U}}{dx} + \frac{\bar{U}}{h} \frac{dh}{dx} = 0, \quad (5)$$

$$\bar{U} \frac{d\bar{U}}{dx} = -\frac{c_f}{h} \bar{U}^2 - g \frac{dh}{dx}. \quad (6)$$

Eliminating the velocity gradient gives us an estimate of the free-surface slope.

$$-\frac{dh}{dx} = c_f \frac{1}{gh/\bar{U}^2 - 1}, \quad (7)$$

where g is the gravitational acceleration.

Figure 3 shows the measured water depths compared with the expected ones, calculated according to Eq. (7). The friction coefficients obtained with Eq. (4) are based on the mean velocity averaged over the high and low velocity sides, and are given in Table I. Those values are used throughout this paper. Figure 3 shows a decrease of the water depth in accordance with theory. Apart from measurement errors the variation of the water depth which is of the order of 1 mm, is caused by unevenness of the flume bottom. This is most obvious at 2 m. The water depth shows hardly any variation with lateral position, although the water level at the high velocity side appears to be on average of the order of 0.1 mm higher than at the low velocity side.

The decrease of the water depth is related to a slight increase with downstream distance of the mean velocity in the flume. The small variation of the mean flow velocity over the length of the flume (less than ten percent) justifies the use of a single friction coefficient for each mixing layer. The geometry of the flow establishes that the lateral variation of the water level is always small with respect to the free-surface slope in streamwise direction. Both the high and the low velocity side of the flume are, therefore, driven by the same forcing while the bottom friction is larger for the high

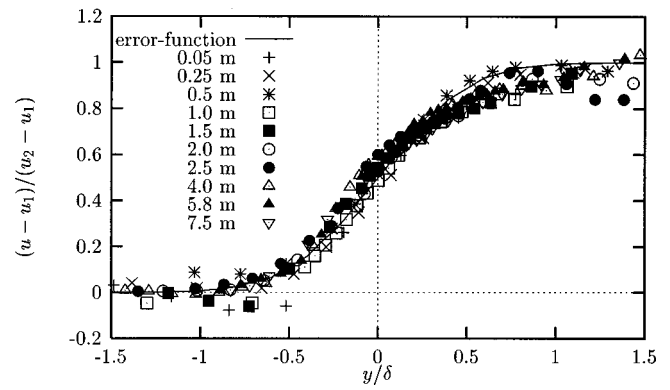


FIG. 4. Mean streamwise velocities vs lateral distance. Lateral distances are scaled with the mixing layer width δ . Water depth is 42 mm.

velocity side. This causes the velocity difference between the streams to decrease, i.e., the slowest stream is accelerated and the fastest one decelerated.

Continuity requires that in a flume of limited width the high-velocity stream broadens at the expense of the width of the low velocity stream. These changes in the two streams lead to a shift of the position of the mixing layer center irrespective of the development of the mixing layer itself.

A. Velocity measurements

The development of the mixing layers is analyzed using lateral profiles of the mean streamwise velocity components. Velocities are measured in the upper part of the flow, away from the bottom 1 cm beneath the free surface. The profiles are collected in Figs. 4 and 5. The lateral coordinate y is scaled with the mixing layer width δ and the streamwise velocity with the velocity difference between the undisturbed flows, see Table II. The mixing layer width is determined from the data as the velocity difference between the two streams divided by the velocity gradient at the center. As a guide to the eye an error-function profile is drawn in that same figure indicating the shape of the self-similar solution as expected for a deep water mixing layer. Although most of the data collapse on the error-curve some scatter remains. This is partly due to the influence of the boundary layer that has developed at the splitter plate and is most prominent at

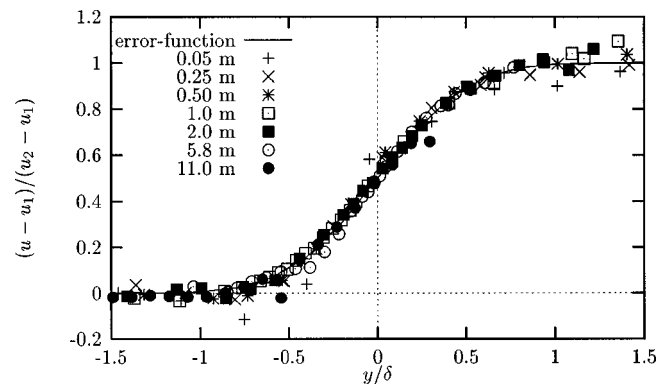


FIG. 5. Mean streamwise velocities vs lateral distance. Lateral distances are scaled with the mixing layer width δ . Water depth is 67 mm.

TABLE II. Velocities on both sides of the mixing layer at the various downstream positions.

x (m)	42 (mm) depth			67 (mm) depth		
	u_1 (m/s)	u_2 (m/s)	λ	u_1 (m/s)	u_2 (m/s)	λ
0.05	0.11	0.23	0.36	0.14	0.32	0.40
0.25	0.11	0.23	0.36	0.14	0.32	0.39
0.5	0.11	0.23	0.35	0.15	0.32	0.38
1.0	0.11	0.22	0.34	0.15	0.32	0.38
1.5	0.12	0.22	0.31			
2.0	0.12	0.21	0.27	0.16	0.32	0.35
2.5	0.13	0.21	0.25			
4.0	0.15	0.20	0.16			
5.8	0.16	0.20	0.12	0.18	0.31	0.27
7.5	0.17	0.20	0.09			
11.0				0.21	0.30	0.19

small downstream distances, and due to possible inhomogeneities in the incoming flow. Moreover the 42 mm case exhibits a systematic deviation from the error profile at the high velocity side of the mixing layer. The bottom friction causes a deceleration of the high velocity side and an acceleration of the low velocity side. This results in a broadening of that part of the flow which has a velocity larger than the mean value and a narrowing of the slower part. In the curves of Figs. 4 and 5 this comes to expression in an asymmetry where the low velocity side of the profile is compressed and the high velocity side is stretched. This effect is more clear in the case of a smaller water depth where the bottom friction has more effect.

From the scaling used in the previous figures the development of the mixing layer width is obtained, Fig. 6. It shows that both mixing layers start to grow at approximately the same rate, only differing due to the inequality of the initial value of λ . The initial growth rate corresponds with that of a deep water mixing layer [drawn according to Eq. (2) as straight dashed lines]. The virtual origin of the growth curves lies slightly upstream of the end of the splitter plate, 0.25 m for the 67 mm case and 0.15 m for the 42 mm case corresponding to an initial mixing layer width at the apex of the splitter plate of 0.023 and 0.012 m, respectively. This is caused by the boundary layer that has developed along both

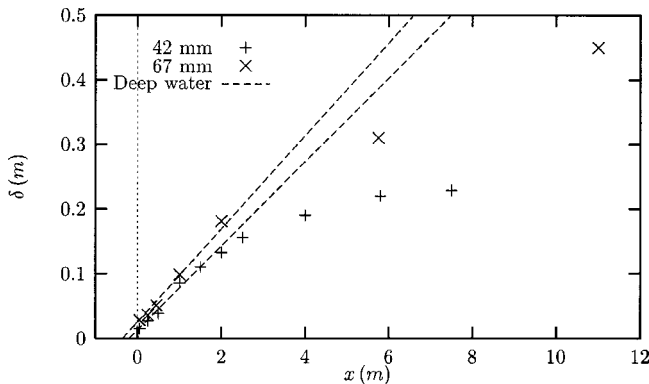


FIG. 6. Mixing layer width vs downstream distance obtained from the profiles of mean streamwise velocity.

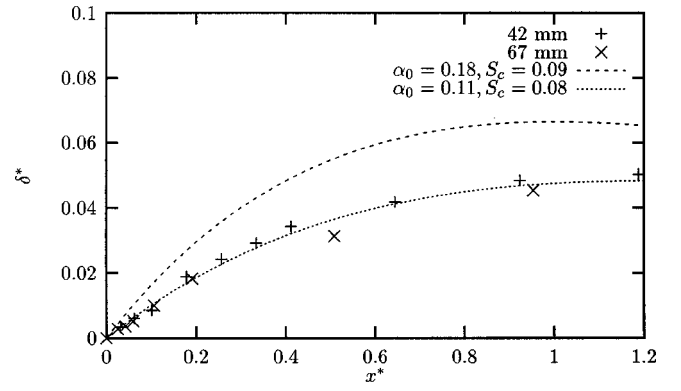


FIG. 7. Mixing layer width vs downstream distance with variables scaled according to Chu & Babarutsi.

sides of the splitter plate. Further downstream the growth rate starts to decrease as a consequence of bottom friction.

According to Chu and Babarutsi⁷ the mixing layer growth can be scaled using the friction length $h/2c_f$ as a characteristic distance. The factor of 2 used here originates from our definition of c_f which differs by a factor of 2 from the definition used by Chu and Babarutsi. In Fig. 7 the dimensionless growth of the two mixing layers with $\delta^* = \delta 2c_f / (h 2\lambda_0)$ and $x^* = x 2c_f / h$ is shown together with the curve obtained with the integral analysis by Chu and Babarutsi (CB).⁷ In this integral analysis they predict the mixing layer growth rate from the independent development of the high and low velocity side of the mixing layer in the presence of friction. This growth rate is assumed, like in Eq. (2), to be proportional to the dimensionless velocity difference λ . The influence of friction comes to expression in the constant of proportionality α :

$$\alpha = \alpha_0 \left(1 - \frac{S}{S_c} \right) \quad \text{for } S < S_c, \quad (8)$$

while for values of S larger than S_c the growth stops, i.e., $\alpha = 0$. Thus in addition to the decrease of λ the bottom friction has its effect on the mixing layer growth rate through S . Using the above mentioned scaling with the c_f values of Table I the experimental data coincide reasonably well on a single curve that can be approached by the theoretical curve with parameters adjusted to $\alpha_0 = 0.11$ and $S_c = 0.08$. For deep-water the growth rate of Eq. (2) gives a value of $\alpha_{dw} = 0.09$ which is close to the 0.11 found here.

The curve that fits the present data deviates considerably from the Chu and Babarutsi data as given in the same Fig. 7 with $\alpha_0 = 0.18$ and $S_c = 0.09$. The initial growth rate of the present data is in reasonable agreement with the predictions for a deep water mixing layer and does not exhibit the doubled spreading rate as found by Chu and Babarutsi. Furthermore, the maximum width the mixing layer can attain in our case ($\delta^* = 0.045$) is smaller than in the CB case ($\delta^* = 0.066$). As already mentioned above, the flow conditions at the splitter plate are of great importance for the further development of the mixing layer. At this point the most important differences between the experimental setups exist. The inlet conditions in the present setup are such that the

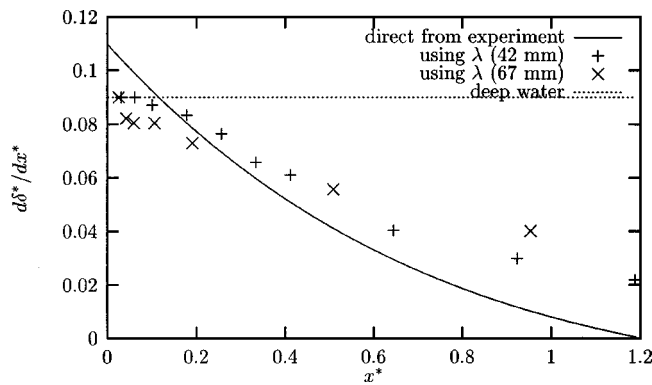


FIG. 8. Mixing layer growth rate vs downstream position. The growth rate obtained from the fit of the previous figure (solid line) is compared with that of a deep-water mixing layer (dotted line) and with the estimates using Eq. (1) with the varying values of λ from Table II as found in the experiments (symbols).

inlet length is sufficient for a full development of the boundary layers at the bottom of the flume and at the splitter plate. This is in contrast with the Chu and Babarutsi setup where the inlet section is much shorter and the contraction, where the flow is still accelerated, ends just before the end of the splitter plate. These differences in the inlet conditions might explain the different development of the mixing layers in both cases (see, e.g., Bell and Mehta¹⁴).

From the smooth curve, through the data of Fig. 7, the growth rate $d\delta^*/dx^*$ can be determined by differentiating it with respect to the scaled downstream position. In Fig. 8 the thus obtained growth rate is compared with the predictions according to Eq. (2) with $\alpha=0.09$ and using values of λ that correspond to the development of the two undisturbed streams. It is seen from this figure that the growth rate that is found in the experiments is not sufficiently explained by the variation of λ alone. In both cases the observed growth rate, represented by the solid line, decreases faster than one would expect from the decrease in velocity difference and the associated decrease of λ , represented by the symbols. The additional effect of bottom friction is the stabilization of the shear layer. The extra dissipation in the bottom boundary layer thus leads to a suppression of the growth of the Kelvin–Helmholtz instabilities in the mixing layer.

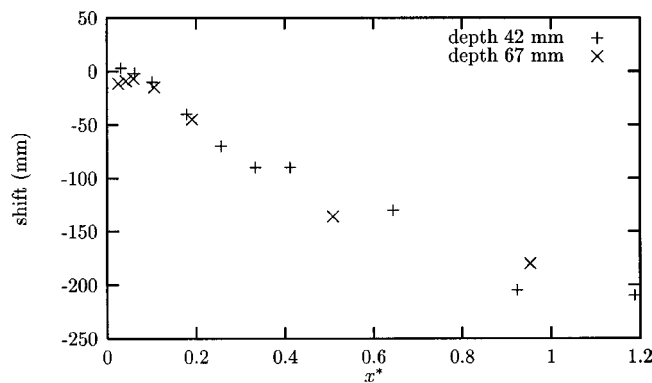


FIG. 9. Lateral shift of mixing layer center.

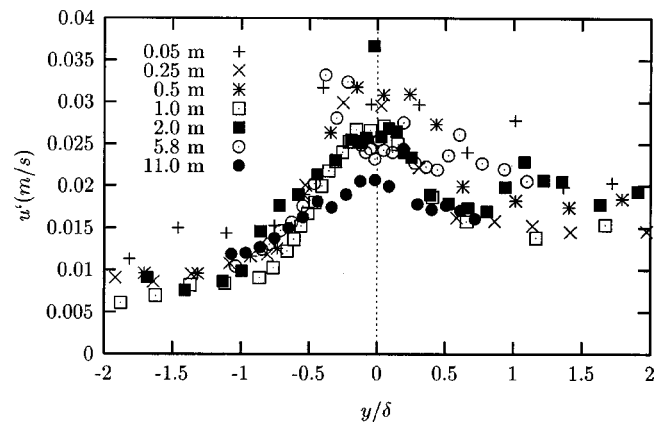


FIG. 10. Profiles of streamwise turbulence intensities at various downstream positions. The lateral distance is scaled with the mixing layer width, water depth 67 mm. The flow conditions corresponding to the positions given in the legend are summarized in Table II.

As a consequence of mass conservation the decrease of the velocity difference, which is most pronounced in the 42 mm case, is causing a shift in the lateral position of the mixing layer center towards the low velocity side of the flume. In Fig. 9 the lateral displacement of the mixing layer center is depicted for both mixing layers. Since the shift is indirectly caused by the bottom friction in streamwise direction the downstream distance is scaled using the friction coefficients from Table I. The data appear to coincide on the same curve. The mixing layer shift can only be established by a small lateral pressure gradient. The water level of the high velocity side should, therefore, be slightly elevated with respect to the low velocity side, which was already concluded from Fig. 3.

The turbulence intensities measured in both mixing layers show characteristic differences. The 67 mm case exhibits a rather constant profile for the streamwise u' , and lateral v' components, Figs. 10 and 11. The maximum values of the curves are in agreement with those obtained in plane mixing layers.²⁰ In this case the decrease of the velocity difference is small and only at large distances downstream a decrease in the turbulence intensity is found. If all the turbulent kinetic

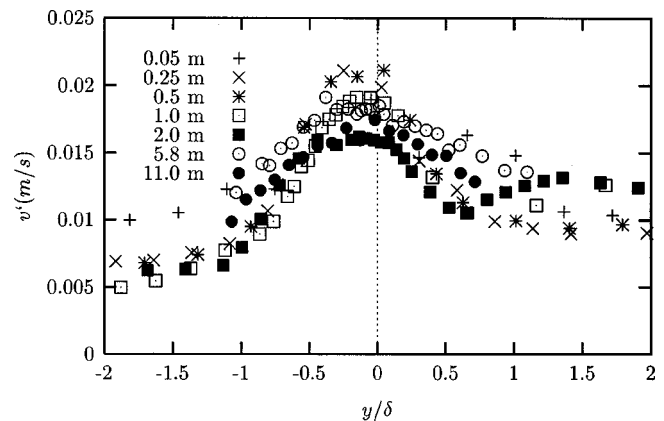


FIG. 11. Profiles of spanwise turbulence intensities at various downstream positions. The lateral distance is scaled with the mixing layer width, water depth 67 mm.

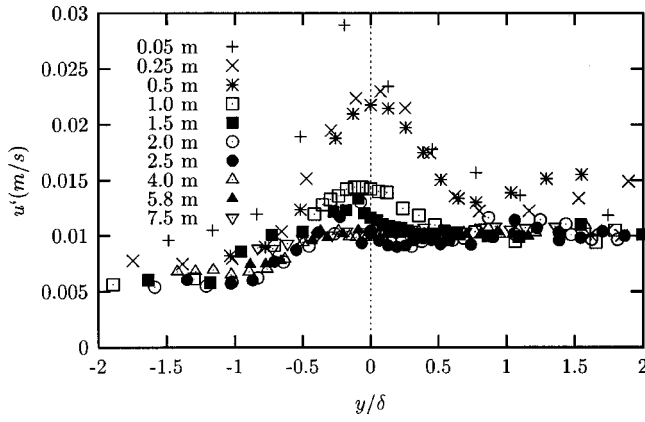


FIG. 12. Profiles of streamwise turbulence intensities at various downstream positions. The lateral distance is scaled with the mixing layer width, water depth 42 mm. The flow conditions corresponding to the positions given in the legend are summarized in Table II.

energy in the flow would have been produced locally one would expect a stronger decrease with downstream distance of the turbulence intensity in the center of the mixing layer. Apparently part of the turbulent fluctuations, presumably the large scales, are advected from upstream positions. The 42 mm case exhibits quite a different behavior (see Figs. 12 and 13). The enhanced turbulence intensity in the center of the mixing layer starts to decrease rapidly beyond 0.5 m and has virtually disappeared at 7.5 m. Looking at the scaled plot of the mixing layer growth (Fig. 7) it can be concluded that despite the fact that the mixing layer width scales properly using δ^* and x^* , the physical processes that take place appear to be essentially different.

The same differences can be found in the transverse profiles of the Reynolds stress in the mixing layer, Figs. 14 and 15. The 67 mm $u'v'$ -correlation has the same order of magnitude as the turbulent kinetic energy indicating a considerable exchange of momentum over the mixing layer. The Reynolds stress is somewhat smaller further downstream. In the 42 mm case however the $u'v'$ -value decreases much faster, in accordance with the strongly reduced turbulent kinetic energy. One of the requirements of a self similar mix-

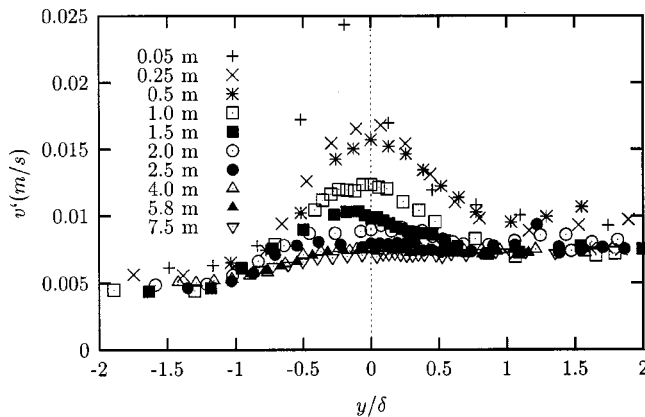


FIG. 13. Profiles of spanwise turbulence intensities at various downstream positions. The lateral distance is scaled with the mixing layer width, water depth 42 mm.

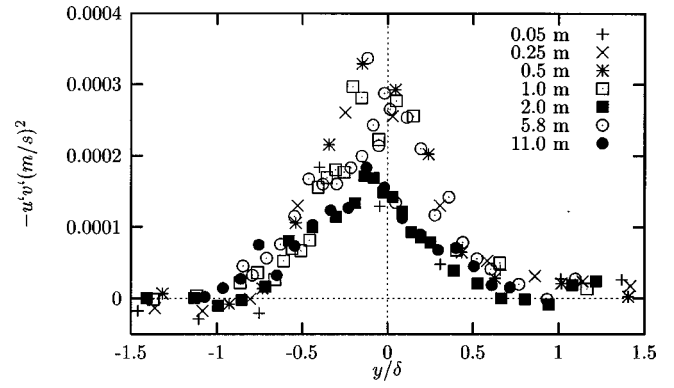


FIG. 14. Lateral profiles of Reynolds stress at 67 mm water depth.

ing layer is that the mixing length for momentum exchange is proportional to the mixing layer width. The mixing length l_m can be estimated from $u'v'$ according to

$$\frac{-u'v'_{\max}}{(u_2 - u_1)^2} = \left(\frac{l_m}{\delta}\right)^2. \quad (9)$$

When the large turbulent structures contribute most to the lateral exchange of momentum and when they grow proportionally with the mixing layer width, the right-hand-side of this equation should be constant. For the 67 mm case this constant is about 0.01, for 42 mm depth it decreases from 0.010 to 0.004. In the latter case the mixing layer contains no strong and frequent large structures that transport momentum over a distance of the same order of magnitude as the mixing layer width. This indicates that the effective mixing length does not grow proportionally to the mixing layer width, but reduces to the order of the water depth. The turbulence becomes dominated by the bottom friction and only little influence is experienced from the lateral velocity gradient. It will be shown in the next paragraphs that these different mixing layer properties can be attributed to the development of the large eddies in the mixing layer.

B. Structures

The large structures that emerge in the mixing layer are recognized through a correlation that extends over a large time span. The autocorrelation function of the velocity fluctuations in lateral direction $R_{vv}(\tau)$ is defined as

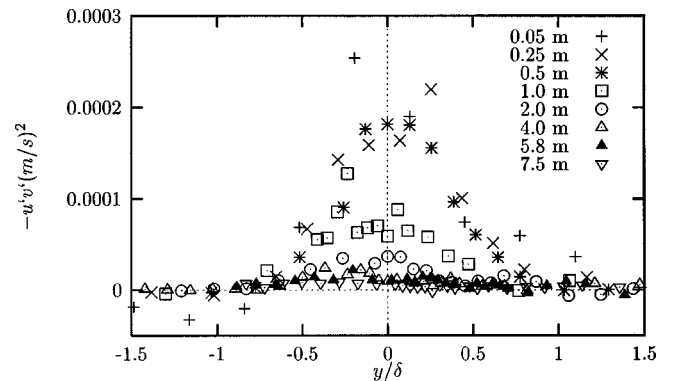


FIG. 15. Lateral profiles of Reynolds stress at 42 mm water depth.

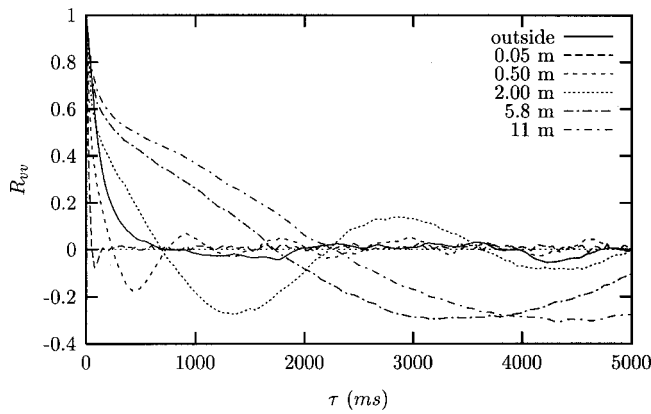


FIG. 16. Autocorrelation functions of spanwise velocity fluctuations outside the mixing layer at the low velocity side and at the center of the mixing layer 0.05, 0.50, 2.00, 5.8, and 11.0 m downstream of the splitter plate 55 mm from the bottom water depth 67 mm.

$$R_{vv}(\tau) = \frac{\langle v(t_0) \cdot v(t_0 + \tau) \rangle}{(\langle v^2(t_0) \rangle \langle v^2(t_0 + \tau) \rangle)^{0.5}}, \quad (10)$$

where the brackets $\langle \rangle$ denote averaging over all values of t_0 .

The differences between the cases with two different depths are clearly visible in Figs. 16 and 17. The 67 mm case shows the presence and growth of large coherent structures that lead to a strong modulation in the correlation function at downstream positions beyond 0.5 m. Comparing the data with the correlation function obtained outside the mixing layer it is seen that at small downstream distances where the mixing layer width is smaller than the water depth, the correlation falls off much faster, demonstrating that the initial part of the mixing layer contains on average much smaller structures than the free stream outside the mixing layer. For the positions further downstream at small values of τ in Fig. 16 a clear transition can be observed where the contribution of the small scale turbulence disappears and only large scale correlation remains. From this figure the disparate time scales of the small and large scale turbulence, of the order of 0.1 and 10 s, respectively, can be noticed. The characteristic time of the modulation is related to the width of the mixing

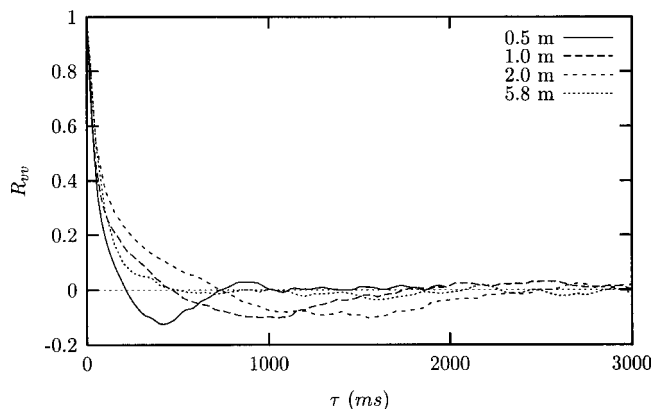


FIG. 17. Autocorrelation functions of spanwise velocity fluctuations in the center of the mixing layer 0.5, 1, 2, and 5.8 m downstream of the splitter plate at 33 mm above the bottom, water depth 42 mm.

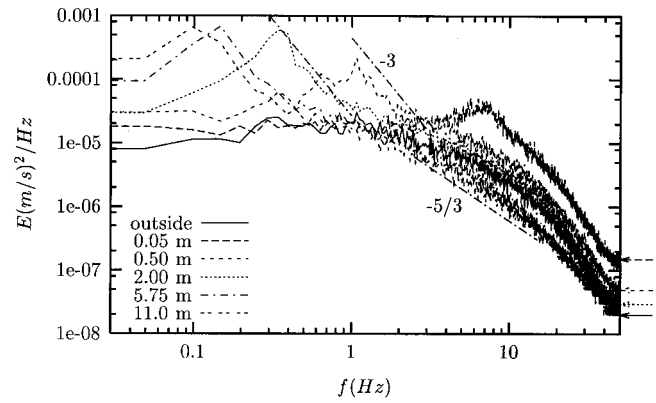


FIG. 18. Power-density spectra of spanwise velocity fluctuations in the center of the mixing layer at various downstream positions, water depth 67 mm. Arrows at the right-hand-side of the graph point to the correspondingly labeled curves.

layer, while its amplitude extrapolated to $\tau=0$ indicates the relative contribution of the large eddies to the total turbulent kinetic energy. The strong modulation that remains significant for several tens of seconds is completely lost in the shallow 42 mm case. In Fig. 17 only a negative loop can be found in the correlation function, with a decreasing amplitude. At 5.8 m the correlation shows no signs of large scale coherence and has become similar to the one outside the mixing layer. Apparently the enhanced dissipation caused by the bottom friction destroys the coherence in the large structures while production due to the lateral shear is not sufficient to support the structures. In the most shallow case the mixing layer becomes “stable,” the large instabilities have disappeared and the growth of the mixing layer has virtually stopped.

C. Spectral analysis

The data that were used for the correlation functions have also been used for determination of the power density spectra of Figs. 18 and 19. The large turbulence structures that are present in the 67 mm case after a certain distance from the splitter plate, yield a definite peak in the power density spectrum, Fig. 18. The amplitude gradually increases

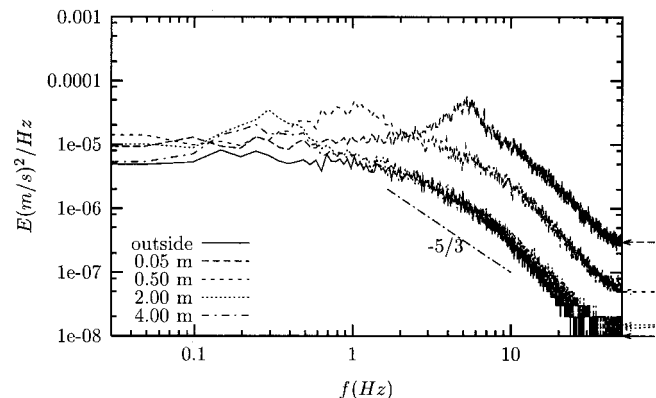


FIG. 19. Power density spectra for velocity fluctuations in spanwise direction for the 42 mm water depth. Arrows at the right-hand-side of the graph point to the correspondingly labeled curves.

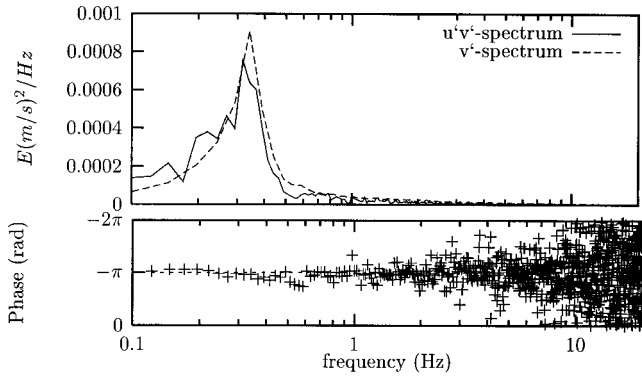


FIG. 20. Cross-power-density spectrum (upper panel) for velocity fluctuations and phase relation (lower panel) for the u' and v' components, 67 mm water depth, 2 m downstream.

and the frequency where the maximum is attained shifts towards lower values with downstream position, corresponding to larger structures. The high-frequency side of all the peaks has a slope of approximately -3 , which may indicate that the large turbulence structures possess two-dimensional characteristics.²¹ The peak height initially increases and stabilizes after 6 m. In the 42 mm case (Fig. 19) a similar peak can be distinguished. The peak amplitude, however, is much smaller and decreases rapidly with downstream distance. Beyond 4 meters the peak has virtually disappeared, obviously in accordance with the correlation functions of Fig. 16.

It is important to note that two mixing layers with initial conditions that, apart from the water depth, differ only slightly exhibit such essentially different behavior. The initial growth rate is the same for both mixing layers and the further development of the mixing layer width appears to scale properly by using the concept of a bottom friction number. The coherence and length scales that are found in both mixing layers, however, are in great contrast. In terms of the bottom friction number the circumstances at 11 m from the splitter plate with 67 mm water depth, and at 4 m with 42 mm depth, are comparable, $S \approx 0.05$. A similarity that, however, cannot be recognized in the turbulence structures.

At the high frequency side of the spectra a gradual decrease of the energy density can be observed. This decrease does not properly follow the $-5/3$ slope that is known from flows with a large inertial subrange. The Reynolds numbers of the present experiments are too small to exhibit this behavior.

In order to ensure that the large turbulence structures are transferring momentum over the mixing layer, cross-spectra have been calculated using the u' and v' data measured at a single point in the mixing layer. In addition to the amplitude for the different frequency components of $u'v'$ also the phase relation between u' and v' is obtained. Figure 20 shows an example of how the main contribution to the Reynolds-stress is related to the motion at low frequencies. The peaks in the $u'v'$ -spectra have their maximum at the same frequencies as in the v'^2 -spectra. The phase relation between u' and v' consequently yields a value of $-\pi$ for the low frequencies, while at the higher frequencies, the phase angles are distributed randomly. The point beyond

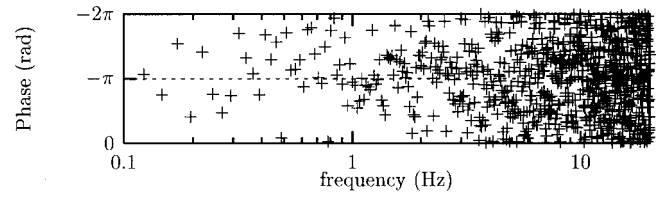


FIG. 21. Example of randomly distributed phase relation between u' and v' outside the mixing layer.

which the phase relation becomes random, is related to the position in the spectrum of the high frequency side of the peak, i.e., with a peak shifting toward lower frequencies this point is shifting proportionally. For comparison the phase relation outside the mixing layer is depicted in Fig. 21, where the phase relation is random in all frequencies. The substantial contribution to the Reynolds-stress in the horizontal plane is, therefore, stemming from the frequency components that are related to the visible peaks in the powerspectra. In the 42 mm case at 2 m downstream there are peaks visible in the v' and the $u'v'$ -spectra (Fig. 22) with amplitudes more than an order of magnitude smaller than in the previous figure and still the same phase difference is apparent. Only further downstream at 4 m with no distinguishable peak present, the phase relation has disappeared corresponding to the virtually zero Reynolds stress (see also Fig. 15).

D. Vertical extension of structures

The coherence in the large structures and their two-dimensional characteristics can be further analyzed by studying the correlation between velocities at different elevations above the bottom. The correlations are defined according to

$$R_{vv}(\tau; z_0, z) = \frac{\langle v(z_0, t_0) \cdot v(z, t_0 + \tau) \rangle}{(\langle v^2(z_0, t_0) \rangle \langle v^2(z, t_0 + \tau) \rangle)^{0.5}}, \quad (11)$$

where $v(z_0)$ denotes the instantaneous local lateral velocity measured by the stationary reference probe and $v(z)$ the velocity at the displaced probe (Fig. 2). The brackets $\langle \rangle$ denote averaging over time.

In a previous paper⁶ it was shown that in the 67 mm case in the first two meters the coherence in vertical direction

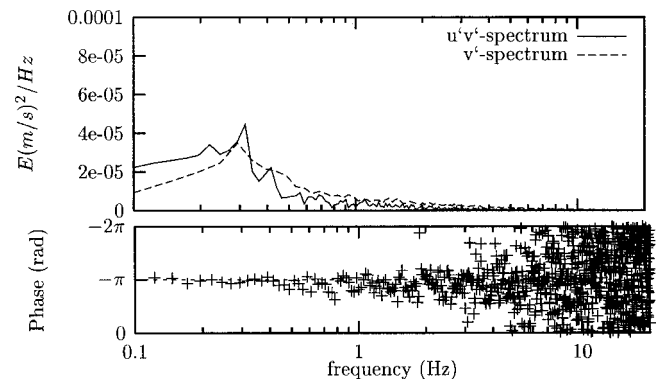


FIG. 22. Cross-power-density spectrum (upper panel) for velocity fluctuations and phase relation (lower panel) for the u' and v' components, 42 mm water depth, 2 m downstream.

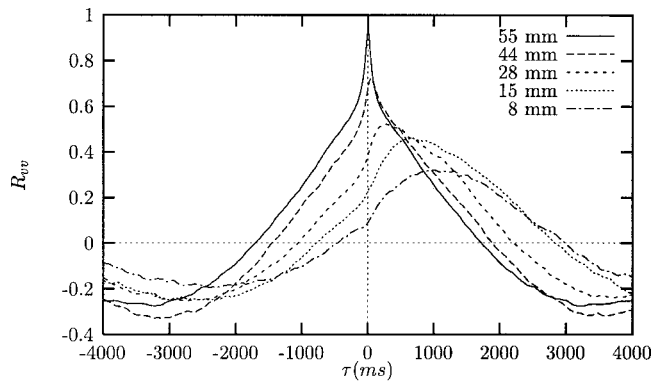


FIG. 23. Time-shifted cross-correlations of LDA-signals obtained at different depths, 6 m downstream of the splitter plate. Reference point is held at 55 mm from bottom, displaced point is located as indicated in the legend, water depth 67 mm.

grows in strength and in size. Beyond the first two meters the correlation is maintained as is shown in Fig. 23 obtained at 5.8 m and in Fig. 24 at 11 m. The amplitudes of the curves indicate that the energy content of the large eddies decreases only slightly in approaching the bottom. Due to the velocity gradient in the flow the maximum of the cross correlation is shifted with respect to $\tau=0$. This indicates that the quasi-two-dimensional eddies extend from the free surface to the bottom with their axes tilted with respect to the vertical direction. Compared with the correlation functions obtained outside the mixing layer as displayed in Fig. 25 the substantial differences are clear. Together with the rapidly vanishing correlation in time (as shown also in Fig. 16) the coherence outside the mixing layer also disappears with a short vertical displacement of about 2 cm.

A similar behavior is found for the more shallow 42 mm case in Figs. 26 and 27, where altered scales for both axes were used to enlarge small differences. The weak coherence as seen in the autocorrelation functions of Fig. 17 is reflected in the spatial correlation in the vertical direction. The curves in Fig. 26 obtained at 2 m downstream of the splitter plate have the same characteristics as those at 4 m, Fig. 27. In the former one the presence of large structures is visible through the larger width of the peaks and the more pronounced nega-

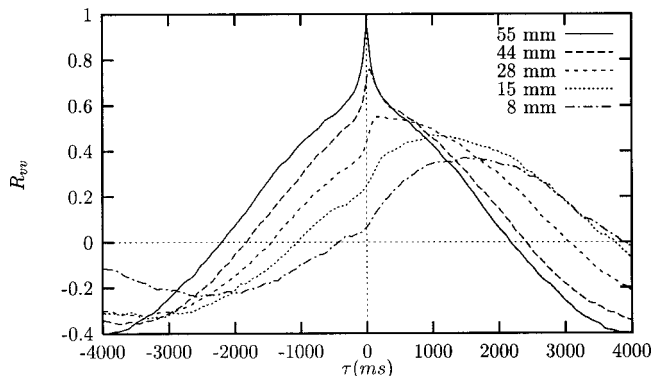


FIG. 24. Time-shifted cross-correlations of LDA-signals obtained at different depths, 11 m downstream of the splitter plate. Reference point is held at 55 mm from the bottom, displaced point is located as indicated in the legend, water depth 67 mm.

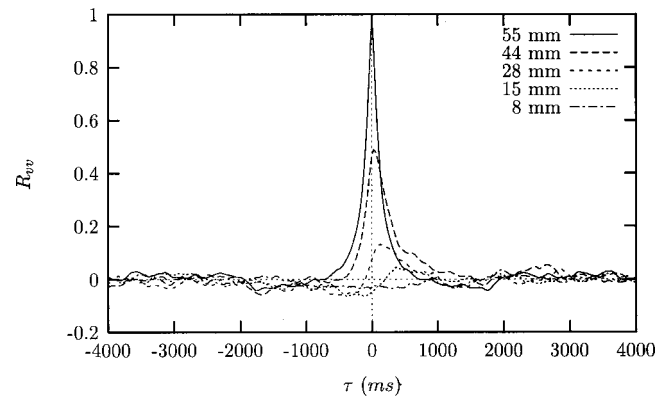


FIG. 25. Time-shifted cross-correlations of LDA-signals of the spanwise component obtained at different depths, outside the mixing layer at the low velocity side. Reference point is held at 55 mm from bottom, displaced point is located as indicated in the legend. Curves are obtained from a 10 min signal with a sampling rate of 100 Hz, water depth 67 mm.

tive loops in the “33” and “25 mm” curves. This confirms the idea that bottom friction and the associated three-dimensional turbulence are dominant in this case and large structures of the size of the mixing layer width are nearly absent.

IV. CONCLUSIONS

In this paper we have shown how the development of mixing layers, and the large structures therein, are affected by the shallowness of the flow. The growth rate of the mixing layer width, which is usually a constant for the deep-water mixing layers, decreases due to the effects of bottom friction in two ways. First, the constant free surface slope in combination with the bottom friction causes the velocity difference between the two ambient stream to diminish and thus the driving force of the mixing layer growth. Second, instabilities that emerge in the mixing layer do not grow fast enough due to the hindrance of bottom friction.

A comparison with experiments on shallow mixing layers by Chu and Babarutsi⁷ shows no proper agreement. Although a scaling of the data, taking into account the bottom friction, gave good results, the absolute data differed sub-

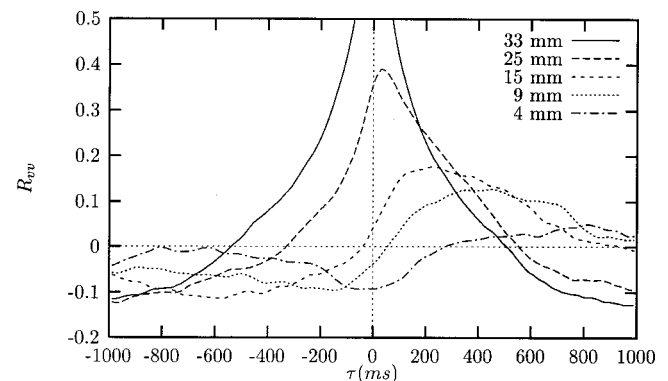


FIG. 26. Time-shifted cross-correlations of LDA-signals obtained at different depths in the mixing layer 2.0 m downstream from the splitter plate. Reference point is held at 33.0 mm from bottom, displaced point is located as indicated in the legend, water depth 42 mm.

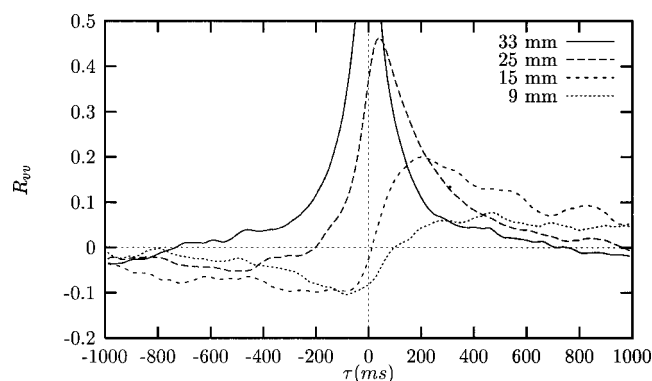


FIG. 27. Time-shifted cross-correlations of LDA-signals obtained at different depths, 4.0 m downstream of the splitter plate. Reference point is held at 33 mm from bottom, displaced point is located as indicated in the legend, water depth 42 mm.

stantially. The initial growth rate and the maximum obtainable mixing layer width in the presence of bottom friction are much larger in the experiments of Chu and Babarutsi.⁷ The differences in the results are attributed to the differences in experimental conditions. It is known from experiments on plane mixing layers that the conditions at the end of the splitter plate can have a dominant effect on the further development of the mixing layer.¹⁴

The development of the large structures in the mixing layer depends on the development of the ambient streams but is also highly affected by the bottom friction. There appears to be a critical point where bottom friction becomes dominant, corroding the large coherent structures that can no longer be sustained by the lateral shear. Although the concept of a bed friction number which covers these phenomena theoretically, leads to a proper scaling of the global results, the details of the large eddies in the two mixing layers as studied in this article are essentially different. In the most shallow case the large coherent structures, initially present in the mixing layer disappear completely, while the bed friction number in this case is comparable with that of the deeper mixing layer where the large structures are dominant. Perhaps a further classification of mixing layer stability is necessary.

A proper description of the interaction between the large and small scale motion and the consequences of the bottom friction needs additional information on the turbulence velocities in vertical direction with emphasis on those close to the bottom. The vertical motions have hitherto not received much attention, partly due to the laboriousness of measuring them through the glass bottom of the flume. By adapting the

optical pathways of the laser beams the current setup can in the near future be made suited to perform full three-dimensional velocity measurements.

Furthermore, quantitative visualization techniques like particle image velocimetry are considered, which could reveal more details of the instantaneous structure of the flow field in general and of the dynamics of the large scale eddies in particular.

- ¹C. M. Ho and P. Huerre, "Perturbed free shear layers," *Annu. Rev. Fluid Mech.* **16**, 365 (1984).
- ²V. H. Chu, J. H. Wu, and R. E. Kayat, "Stability in turbulent shear flow in shallow channel," *J. Hydraulic Engineering* **117**, 128 (1991).
- ³D. Chen and G. H. Jirka, "Experimental study of plane turbulent wakes in a shallow water layer," *Fluid Dyn. Res.* **16**, 11 (1995).
- ⁴S. Babarutsi, M. Nassiri, and V. H. Chu, "Computation of shallow recirculating flow dominated by friction," *J. Hydr. Engrg.* **122**, 367 (1996).
- ⁵M. D. J. P. Bijvelds, C. Kranenburg, and G. S. Stelling, "3-d numerical simulation of turbulent shallow-water flow in square harbor," *J. Hydraulic Engineering* **125**, 26 (1999).
- ⁶T. Dracos, M. Giger, and G. H. Jirka, "Plane turbulent jets in a bounded fluid layer," *J. Fluid Mech.* **241**, 587 (1992).
- ⁷V. H. Chu and S. Babarutsi, "Confinement and bed-friction effects in shallow turbulent mixing layers," *J. Hydraul. Engineering* **114**, 1257 (1988).
- ⁸W. S. J. Uijttewaai and J. Tukker, "Development of quasi two-dimensional structures in a shallow free-surface mixing layer," *Exp. Fluids* **24**, 192 (1998).
- ⁹G. L. Brown and A. Roshko, "On density effects and large structure in turbulent mixing layers," *J. Fluid Mech.* **64**, 775 (1974).
- ¹⁰R. D. Moser and M. M. Rogers, "The three-dimensional evolution of a plane mixing layer: pairing and transition to turbulence," *J. Fluid Mech.* **247**, 257 (1993).
- ¹¹G. M. Corcos and F. S. Sherman, "The mixing layer: deterministic models of a turbulent flow. part 1. introduction and the two-dimensional flow," *J. Fluid Mech.* **139**, 29 (1984).
- ¹²A. A. Townsend, *The structure of turbulent shear flow* (Cambridge University Press, Cambridge, 1956).
- ¹³D. Oster and I. Wygnanski, "The forced mixing layer between parallel streams," *J. Fluid Mech.* **123**, 91 (1982).
- ¹⁴J. H. Bell and R. D. Mehta, "Development of a two-stream mixing layer from tripped and untripped boundary layers," *AIAA J.* **28**, 2034 (1990).
- ¹⁵V. H. Chu, J. H. Wu, and R. E. Kayat, "Stability in turbulent shear flow in shallow channel," in *Proceedings of the 20th I.A.H.R. congress, Moscow*, pp. 128–133, 1983.
- ¹⁶D. Chen and G. H. Jirka, "Absolute and convective instabilities of plane turbulent wakes in a shallow water layer," *J. Fluid Mech.* **338**, 157 (1997).
- ¹⁷V. Alavian and V. H. Chu, "Turbulent exchange flow in shallow compound channel," in *Proceedings of the 21th I.A.H.R. congress, Melbourne*, pp. 19–23, 1985.
- ¹⁸D. C. van Senden and J. Imberger, "Effects of initial conditions and Ekman suction on tidal outflows from inlets," *J. Geophys. Res.* **95**, 13373 (1990).
- ¹⁹W. R. Carter, H. A. Einstein, J. Hinds, R. W. Powell, and E. Silberman, "Friction factors in open channels," *J. Hydraulic Div.* **89**, 97 (1963).
- ²⁰I. Wygnanski and H. E. Fiedler, "The two-dimensional mixing region," *J. Fluid Mech.* **41**, 327 (1970).
- ²¹G. K. Batchelor, "Computation of the energy spectrum in homogeneous two-dimensional turbulence," *Phys. Fluids Suppl.* **II**, 233 (1969).